Nuclear Engineering and Technology 54 (2022) 2367–2375

Contents lists available at ScienceDirect

Nuclear Engineering and Technology

journal homepage: www.elsevier.com/locate/net

Original Article

Physics-based modelling and validation of inter-granular helium behaviour in SCIANTIX

R. Giorgi [a], A. Cechet [a], L. Cognini [a], A. Magni [a], D. Pizzocri [a], G. Zullo [a], A. Schubert [b], P. Van Uffelen [b], L. Luzzi [a, *]

[a] Politecnico di Milano, Department of Energy, Nuclear Engineering Division, via La Masa 34, 20156, Milano, Italy
[b] European Commission, Joint Research Centre (JRC), Karlsruhe, Germany

ARTICLE INFO

Article history:
Received 8 July 2021
Received in revised form
28 December 2021
Accepted 5 January 2022
Available online 8 January 2022

Keywords:
Helium behaviour
Oxide nuclear fuel
Meso-scale modelling
Fuel performance codes
SCIANTIX

ABSTRACT

In this work, we propose a new mechanistic model for the treatment of helium behaviour at the grain boundaries in oxide nuclear fuel. The model provides a rate-theory description of helium inter-granular behaviour, considering diffusion towards grain edges, trapping in lenticular bubbles, and thermal re-solution. It is paired with a rate-theory description of helium intra-granular behaviour that includes diffusion towards grain boundaries, trapping in spherical bubbles, and thermal re-solution. The proposed model has been implemented in the meso-scale software designed for coupling with fuel performance codes SCIANTIX. It is validated against thermal desorption experiments performed on doped UO_2 samples annealed at different temperatures. The overall agreement of the new model with the experimental data is improved, both in terms of integral helium release and of the helium release rate. By considering the contribution of helium at the grain boundaries in the new model, it is possible to represent the kinetics of helium release rate at high temperature. Given the uncertainties involved in the initial conditions for the inter-granular part of the model and the uncertainties associated to some model parameters for which limited lower-length scale information is available, such as the helium diffusivity at the grain boundaries, the results are complemented by a dedicated uncertainty analysis. This assessment demonstrates that the initial conditions, chosen in a reasonable range, have limited impact on the results, and confirms that it is possible to achieve satisfying results using sound values for the uncertain physical parameters.

1. Introduction

The description of helium behaviour in nuclear fuel is of engineering interest: (1) during irradiation, it concurs to the gaseous swelling of the fuel pin and gas release in the free volume of the fuel rod together with xenon and krypton, and progressively becomes dominant (2) during storage, since it is produced in large amounts due to the α-decay of actinides. The importance of helium in dry storage conditions is related to its contribution, together with accumulation of radiation damage [1] to the increase of rod internal pressure [2], potentially concerning for the safety limit imposed in terms of maximum hoop stress in the cladding [3–7]. On one hand, targeting engineering approaches to the verification of the respect of design limits, modelling of helium behaviour and release in dry storage conditions is typically (conservatively) simplified. In their analysis for example, Raynaud and Einziger [8] assumed a constant 5% of release from the fuel, which overestimates the expected helium release at fuel temperature below 650 K. On the other hand, the development of multi-physical, multi-scale strategies for the simulation of fuel rod behaviour in dry storage conditions is arising, involving fuel performance codes supported by neutronic and thermohydraulic simulations [9–12].

In the state-of-the-art models [13–18] used in thermo-mechanical fuel performance codes [19–21], the description of gas and helium behaviour is approached in three sequential steps [22,23]: production, intra-granular evolution [24–27] and inter-granular evolution [28]. The rate-theory model proposed in this work is similarly designed and is intended for application in fuel performance codes, extending the capabilities of currently available models [22]. The focus is on including the physical description of

* Corresponding author.
E-mail address: lelio.luzzi@polimi.it (L. Luzzi).

https://doi.org/10.1016/j.net.2022.01.012

Table 1
Parameters involved in the inter-granular model proposed in this work.

Symbol	Description	Formula	u.o.m.	Reference
D_{ig}	Intra-granular diffusion coefficient	$2.0\cdot10^{-10}\exp(-2.12/kT)$	$m^2\ s^{-1}$	[22,37]
D_{gb}	Inter-granular diffusion coefficient	$10^3\cdot D_{ig}$	$m^2\ s^{-1}$	Present work
g_{gb}	Inter-granular trapping rate	$2\pi D_{gb}N_{gb}/\ln(1/R_{gb}\sqrt{\pi N_{gb}})$	s^{-1}	Present work, [38]
$c_{s,gb}$	Inter-granular helium solubility	$\frac{a}{3}k_H p_{gb}$	at m^{-2}	[10,22–24]
k_H	Henry's constant	$4.1\cdot10^{24}\exp(-0.65/kT)$	at m^{-3} MPa^{-1}	[22,35,39–41]
γ_{gb}	Inter-granular thermal re-solution	$\frac{2\pi D_{gb}}{ln\left(\frac{1}{R_{gb}\sqrt{\pi N_{gb}}}\right)}\frac{a}{3}k_H\frac{kT}{V_{gb}}Z$	s^{-1}	Present work
p_{gb}	Inter-granular helium bubble pressure	$kTZn_{gb}/V_{gb}$	Pa	
Z	Compressibility factor	$(1+y+y^2-y^3)/(1-y)^3$	/	[22,42]
y	Volumetric fraction of gas	$\frac{\pi d^3}{6V_{at}}$	/	[22,42]
d	Hard-sphere diameter	$2.973\cdot10^{-10}\left[0.8414-0.05\,ln\left(\frac{T}{10.985}\right)\right]$	m	[22,42]
F	Fractional coverage	$N_{gb}A_{gb}$	/	[28]
V_{gb}	Average inter-granular bubble volume	$4\phi(\theta)\pi R_{gb}^3/(3sin^3(\theta))$	m^3	[28]
$\phi(\theta)$	Semi-dihedral factor of a bubble	$1-1.5\cos(\theta)+0.5cos^3(\theta)$	/	[28,43]

inter-granular helium behaviour to improve the predicting capabilities of helium evolution in annealing conditions.

The model has been implemented in the meso-scale software SCIANTIX [29], designed for coupling with fuel performance codes. Given the uncertainties involved in the initial conditions for the inter-granular part of the model (i.e., the initial grain-boundary in-bubble helium concentration and the helium single-atom concentration) and the uncertainties that are associated to some model parameters, for which limited lower-length scale information is available (helium diffusivity [30] at the grain boundaries in particular), the results are complemented by a dedicated uncertainty analysis. The model is presented in Section 2, with a description of the various parameter involved. The experimental data and the obtained results are showcased and described in Section 3. The sensitivity analysis on the input parameters is presented in Section 4 and the conclusions are drawn in Section 5.

2. Model description

In line with the fission gas behaviour model of Van Uffelen [31], we assume that helium atoms co-exist in two phases at the grain boundaries. One fraction is dissolved in the grain boundary (c_{gb}), whereas the other part is accumulated in bubbles (m_{gb}). The governing equations for the evolution of the single-atom and the in-bubble helium concentrations at the grain boundaries read:

$$\frac{\partial c_{gb}}{\partial t} = S(1-F) + D_{gb}\nabla^2 c_{gb} - g_{gb}\left(c_{gb}-c_{s,gb}\right) + b_{gb}m_{gb} - \nu_{gb}n_{gb}$$
$$\frac{\partial m_{gb}}{\partial t} = SF + g_{gb}\left(c_{gb}-c_{s,gb}\right) - b_{gb}m_{gb} + \nu_{gb}n_{gb} \quad (1)$$

where S (at m^{-2} s^{-1}) represents the helium source from within the grain, D_{gb} (m^2 s^{-1}) is the inter-granular helium diffusion coefficient, c_{gb} (at m^{-2}) is the inter-granular single atom helium concentration, $c_{s,gb}$ (at m^{-2}) is the solubility of helium at grain boundaries, g_{gb} (s^{-1}) is the trapping rate, b_{gb} (s^{-1}) is the irradiation induced re-solution term, m_{gb} (at m^{-2}) is the helium concentration in inter-granular bubbles, ν_{gb} (bub s^{-1}) is the nucleation term, n_{gb} (at bub^{-1})is the number density of helium atoms per inter-granular bubble and F (/) is the fractional coverage of the grain faces. The fractional coverage

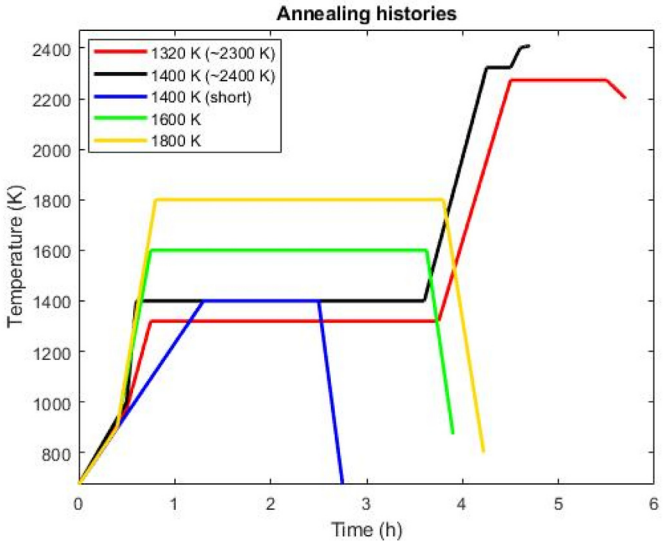

Fig. 1. Temperature histories of the considered annealing experiments considered [36].

acts as a parameter that distributes the helium reaching the grain boundary among the inter-granular bubble and the single-atom contributions.

Some further considerations were made to develop Eq. (1). We assume that at the grain-boundary helium moves on a 2D surface, since the grain boundary thickness is on the order of a nanometre whereas the size of the grain-face is on the order of microns, thus diffusion process acts accordingly. In line with the models for intergranular precipitation of fission gas atoms [32,33], the diffusion of helium on the grain boundary is approximated by the radial component of the cylindrical Laplacian operator, with r (m) being the radial position along the grain face, assumed as circular:

$$D_{gb}\nabla^2 c_{gb} = D_{gb}\frac{1}{r}\frac{\partial}{\partial r}r\frac{\partial}{\partial r}c_{gb} \quad (2)$$

Diffusion of intra-granular helium towards the grain boundary represents the source of helium single-atoms at grain-boundary (S). This makes the grain boundary evolution connected to the intra-granular behaviour.

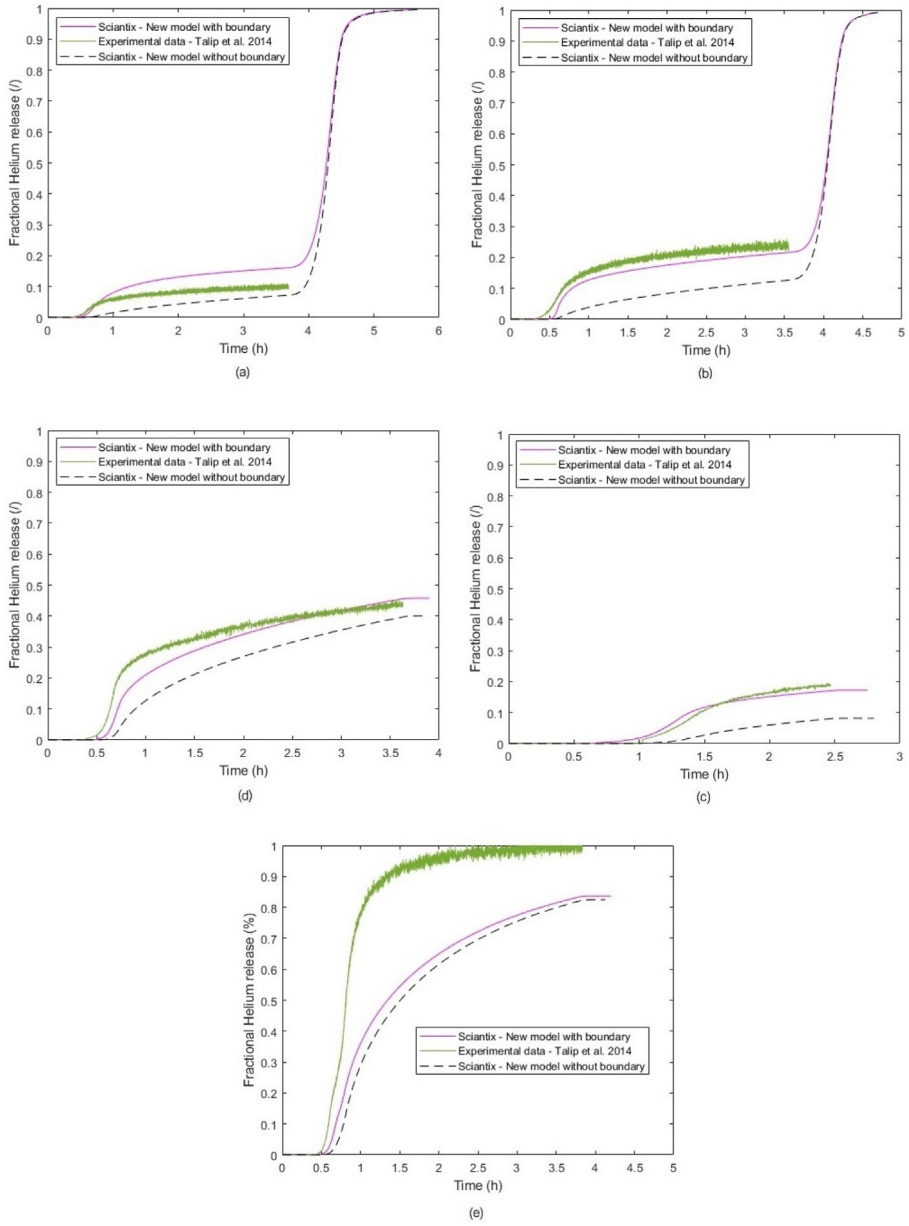

Fig. 2. Comparison of SCIANTIX fractional helium release with experimental data provided by Talip et al. [36] on the history at 1320 K (a), 1400 K (b) 1400 K (short) (c), 1600 K (d) and 1800 K (e). The black dashed line represents the results from Cognini et al. [22] and the purple line the present development including grain boundary treatment. (For interpretation of the references to colour in this figure legend, the reader is referred to the Web version of this article.)

To express S coherently, the intra-granular helium single atom concentration c_{ig} (at m^{-3}) needs to be rescaled on a 2D space by means of the surface-to-volume ratio of the spherical grain which is equal to one third of the spherical grain radius itself, i.e., $c_{ig,gb} = \frac{a}{3}c_{ig}$.where $c_{ig,\,gb}$ (at m^{-2}) is the contribution to grain boundary helium coming from within the grain, a (m) is the spherical grain along which we define the radial coordinate r_*. Thus, the expression of S becomes:

$$S = -\frac{a}{3}D_{ig}\frac{1}{r_*^2}\frac{\partial}{\partial r_*}r_*^2\frac{\partial}{\partial r_*}c_{ig} \tag{3}$$

In Eq. (3), D_{ig} is the intra-granular diffusion coefficient ($m^2\ s^{-1}$). The Laplacian of the source term remains expressed in spherical coordinates because it is a consequence of the intra-granular diffusion mechanism, that we model with the Booth equivalent sphere approach [34]. In analogy with early work on the helium intra-granular model [22], we include the helium solubility at the grain boundaries that follows Henry's law:

$$c_{s,gb} = \frac{a}{3}k_H p_{gb} \tag{4}$$

where k_H (at $m^{-3}\ Pa^{-1}$) is the Henry constant [35], p_{gb} (Pa) is the helium pressure at the grain boundaries and $\frac{a}{3}$ is the surface-to-volume ratio, used again as a conversion factor. The solubility leads to a thermally activated re-solution of the helium single atoms from bubbles of the form:

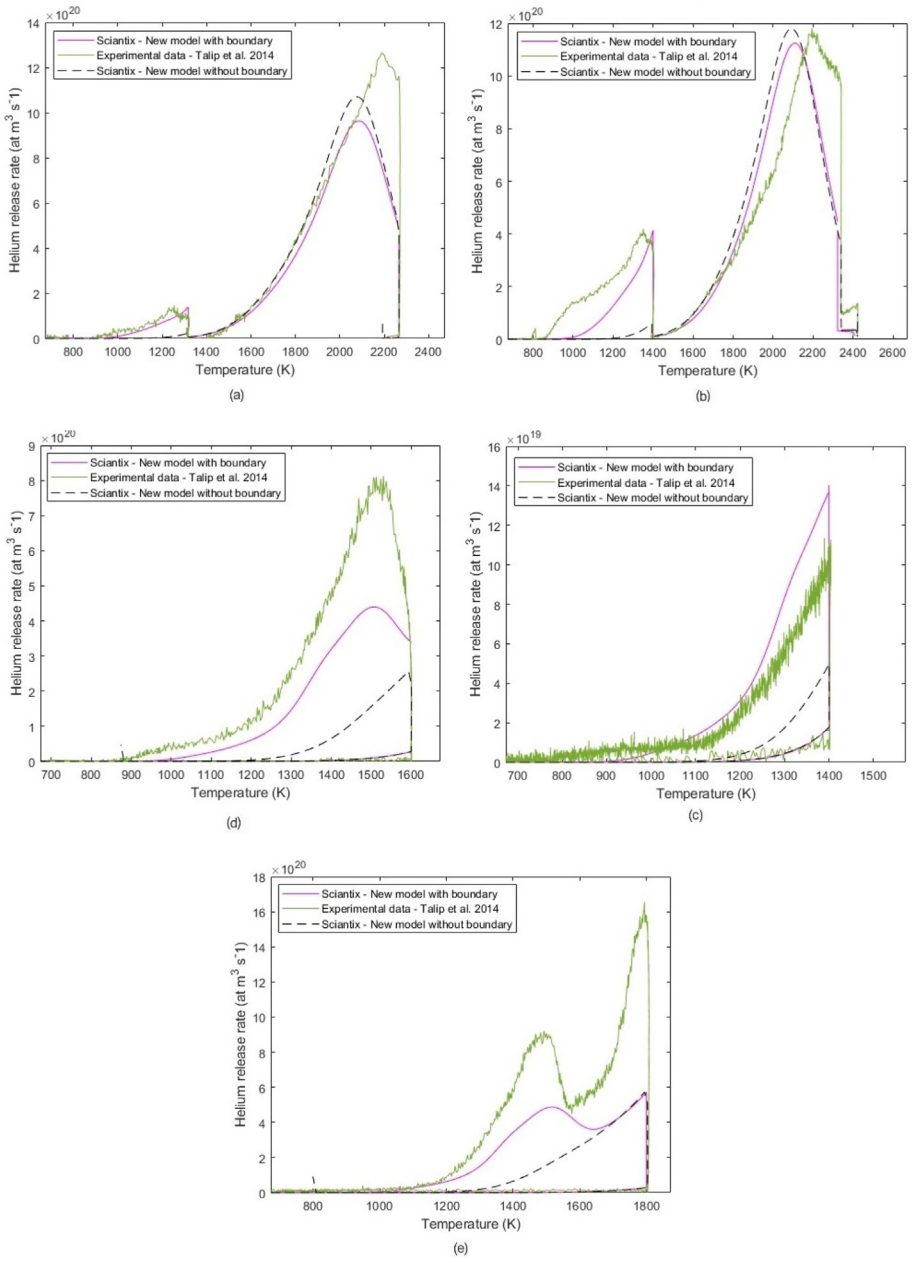

Fig. 3. Comparison of SCIANTIX fractional helium release rate with experimental data provided by Talip et al. [36] on the history at 1320 K (a), 1400 K (b) 1400 K (short) (c), 1600 K (d) and 1800 K (e). The black dashed line represents the results from Cognini et al. [22] and the purple line the present development including grain boundary treatment. (For interpretation of the references to colour in this figure legend, the reader is referred to the Web version of this article.)

$$\gamma_{gb} m_{gb} = g_{gb} c_{s,gb} \tag{5}$$

being γ_{gb} (s^{-1}) the inter-granular thermal re-solution rate.

In annealing conditions, the irradiation induced re-solution rate is null ($b_{gb} = 0\ s^{-1}$) and it is assumed that a bubble population is formed at the first time-step (*one-off nucleation*) and then it evolves along the experiment [22,36]; thus, if we implement Eqs. (2)–(4) into Eq. (1), the inter-granular system of equations become:

$$\frac{\partial c_{gb}}{\partial t} = -\frac{a}{3} D_{ig} \frac{1}{r_*^2} \frac{\partial}{\partial r_*} r_*^2 \frac{\partial}{\partial r} c_{ig}(1-F) + D_{gb} \frac{1}{r} \frac{\partial}{\partial r} r \frac{\partial}{\partial r} c_{gb} - g_{gb} c_{gb}$$

$$+\gamma_{gb} m_{gb} \quad \frac{\partial m_{gb}}{\partial t} = -\frac{a}{3} D_{ig} \frac{1}{r_*^2} \frac{\partial}{\partial r_*} r_*^2 \frac{\partial}{\partial r} c_{ig} F + g_{gb} c_{gb} - \gamma_{gb} m_{gb} \tag{6}$$

These equations are coupled with those defining the model for the intra-granular helium evolution, detailed in Ref. [22]. The various parameters involved in the inter-granular model can be found in Table 1.

3. Results

To validate the model represented by Eq. (1), we compared the SCIANTIX results on fractional helium release and release rate against a set of data collected by Talip et al. [36] during annealing

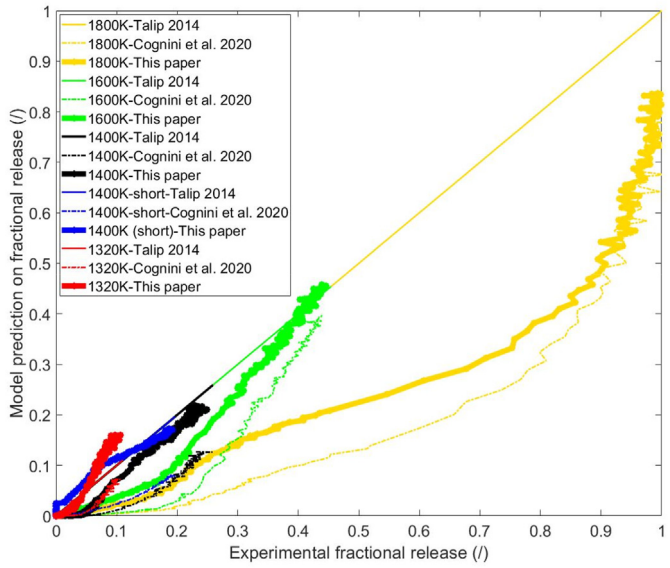

Fig. 4. Statistical comparison of the present model (thick lines) with respect to the intra-granular only model by Cognini et al. (dashed lines). The bisector lines (continuous lines), built using the experimental data, represent the regression lines.

Table 2
Values of statistical R^2 of the fractional release model curves evaluated using the experimental data by Talip et al. [36] as regression line.

Histories	$R^2_{\text{Cognini et al. (2020)}}$	$R^2_{\text{This work}}$
1320 K	0.5532	0.4568
1400 K	0.3373	0.8935
1400 K (short)	0.3410	0.9738
1600 K	0.8675	0.9669
1800 K	0.8028	0.8501

measurements. The experiment was performed on UO_2 samples doped with 0.1 wt% of additive containing 66.7 wt% of $^{238}PuO_2$, whose α-decay produce helium atoms within the sample during an aging period of 15 years in a glovebox with inert atmosphere (N_2). The samples were then annealed in a Knudsen Effusion Mass Spectrometer and helium release was measured using a Quantitative Gas Measurement System (Q-GAMES) [44]. The five annealing temperatures [36] considered in this work are shown in Fig. 1.

All histories are characterized by a heat up ramp of 30 min at 10–20 K min^{-1} with a subsequent hold of the temperature, at a value of 1800 K, for 1–3 h. In three out of five annealing histories, the temperature is decreased to 800 K after the plateau, while in two histories (1320 K and 1400 K) there is a second heat up phase up to 2300–2400 K.

For the considered histories, the behaviour of helium fractional release and helium release rate is reported. The results of the model incorporating the contribution of the grain boundaries are also compared to the previous version of the model (only intra-granular contribution, without any representation of grain-boundary behaviour) and with the aforementioned experimental results [36]. Modelling assumptions, necessary for the set-up of the SCIANTIX simulation are made on the inter-granular helium diffusion coefficient and on the fraction of helium initially considered at grain boundaries. In particular, a reference value of 10% of the helium produced is taken for the fraction of helium initially present at the grain-boundary [30]and the ratio D_{gb}/D_{ig} is assumed to be 10^3 [30].

Fig. 2 and Fig. 3 show that the inclusion of a model treating helium behaviour at the grain boundaries provides a further step to enlighten the physical behaviour of this gas inside nuclear fuel. Looking at the helium fractional release, despite an overestimation on the 1320 K profile, the other graphs show significant improvements, especially on the 1400 K, 1400 K (short), and 1600 K histories. The overestimation for 1320 K is within the acceptance band of a factor 2 applied to fission gas atoms. The release at 1800 K is still underestimated, but this could be due to the uncertainty on the initial values of helium at the grain-boundary. As for the helium release rate, the profiles show an improvement compared to the previous version of the model. The most noticeable observation on this part can be made on the presence of a double peak release rate profile for the 1800 K history. The presence of a peak at a lower temperature, followed by a second at a higher temperature, is consistent with the fact that, as stated by Martin et al. [45,46], the release of helium occurs in two successive stages. The first stage corresponds to the release of helium which is close to the grain boundaries, i.e., along the concentration gradient. The second stage of helium release should occur via the slow re-solution and release of gas atoms trapped within grains. This behaviour is not visible in all the histories because in some of them (namely 1400 K (short) and 1600 K) the maximum temperature reached is not high enough to produce the effect just mentioned. For the 1800 K history it is particularly relevant to predict the double peak since the first one of the two represents the behaviour of helium in the 1600 K history.

Thus, obtaining the same value of release rate in the 1600 K peak and in the 1800 K first peak shows that the model produces coherent results among different histories. Apart from the 1800 K history, a general improvement in the new model estimation of the release rate can be appreciated.

To further show the improvement provided by the inclusion of the inter-granular model in simulating helium behaviour, Fig. 4 is provided. The figure compares the predicting capabilities on the fractional helium release of the new model and the intra-granular only model by Cognini et al. [22] with the experimental results by Talip et al. [36] that are projected on the bisector line of the graph. Notice that the lines representing the experimental data, which are used as regression lines, are actually comprised of the discrete set of data by Talip et al. [36], and this is the reason why the model trends appear noisy. It should also be highlighted a difference from the results presented in Fig. 3: for the histories with a second heat up ramp (namely 1320 K and 1400 K) the models have been interrupted at values of time when the experimental data ended, otherwise, still due to the nature of how the regression lines are built, this further evaluation would lose its meaning. Nonetheless, the results confirm the previously assessed overall improvement of the new model simulating capabilities with respect to the model by Cognini et al. [22]. All the model predicted curves are closer to the experimental regression lines and this improvement is also quantified by means of the R^2 parameter, as can be seen in Table 2.

Thus, helium at grain boundaries plays a relevant role on the overall helium behaviour and the evidence that the proposed model can correctly predict the two stages in which release occurs is a promising achievement.

4. Uncertainty analysis

Given the lack of experimental information on helium at grain boundaries, some assumptions are made on the initial values of some parameters of the model, namely the initial fraction of helium stored at the grain boundaries at the beginning of the annealing test and its distribution among inter-granular bubble and inter-granular single-atom concentrations, together with the diffusivity of helium at the grain boundaries.

The hypothesis of considering an initial portion of the helium produced in the samples at the grain boundaries comes from Martin

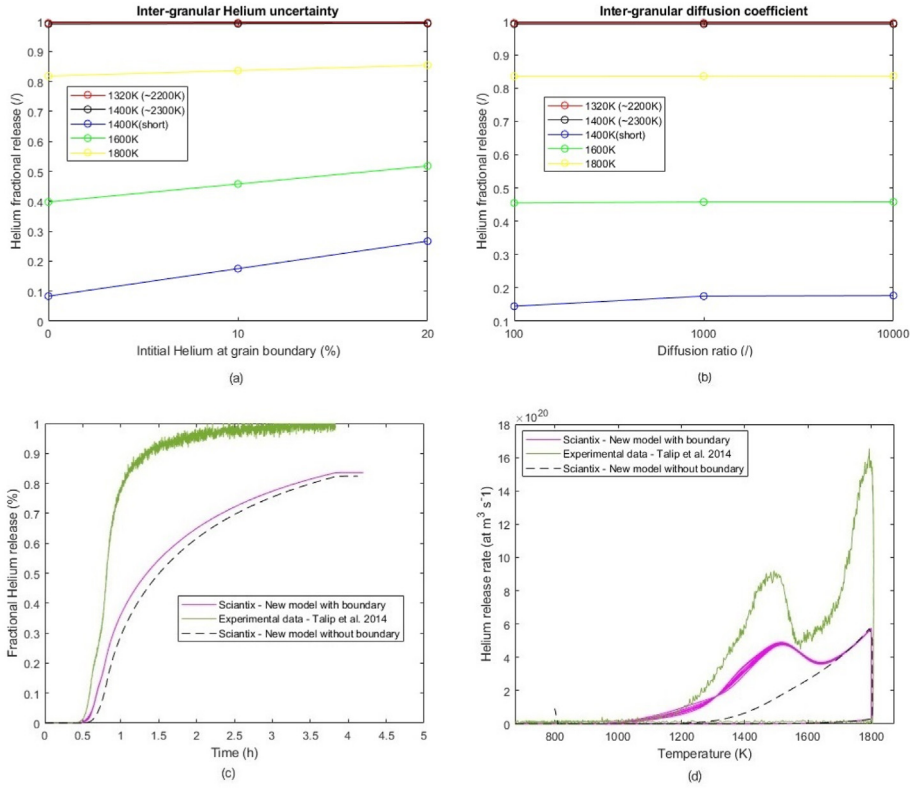

Fig. 5. Effects of the uncertainty analysis on helium release behaviour: (a) effect of the fraction of helium initially present at grain boundaries on the fractional release, (b) effect of the diffusion coefficient on the fractional release, (c) bundle of curves that shows the effects on fractional release of how the fraction of helium initially present at grain boundaries is split between bubbles (100 curves in a range between 0% and 50%) and solution (effect show on 1800 K history), (d) bundle of curves that shows the effects on release rate of how the fraction of helium initially present at grain boundaries is split between bubbles (in a range between 0% and 50%) and solution (effect show on 1800 K history).

et al. [45], who stated that a fraction of the helium initially produced in a sample is close enough to the grain boundaries to be considered in it.[1] As for the exact value of this initial grain boundary contribution, no experimental data are available. To throw light into this fundamental model parameter, mandatory for the initialization of the SCIANTIX simulation, an uncertainty analysis is performed. Since the samples were doped and kept in a controlled atmosphere for 15 years, it is reasonable to assume that, before the annealing procedure, helium is mainly trapped within the grains. For this reason, a fraction of helium between 0% and 20% of the helium produced is initially considered at grain boundaries. The mean value (10%) is assumed as a reference value, showing promising results (as can be seen from Fig. 4). It is possible to see from Fig. 5(a) that, within the chosen range of uncertainty, the effect on the overall release is more relevant when the maximum temperature reached is lower (we recall that the temperature stories labelled with 1320 K and 1400 K are peculiar because the main plateau, which gives the name to the history, does not represent the maximum temperature reached, which is instead about 1000 K higher). This effect can still be explained by referring back to what Martin et al. said on the release phases [45,46]. When the maximum temperatures reached are lower, the bulk of the contribution to the overall release is attributable precisely to the helium initially present at grain boundaries which, being characterized by a diffusion term several orders of magnitude higher than its intra-granular counterpart, is fully released even at lower temperatures. Consequently, the impact of

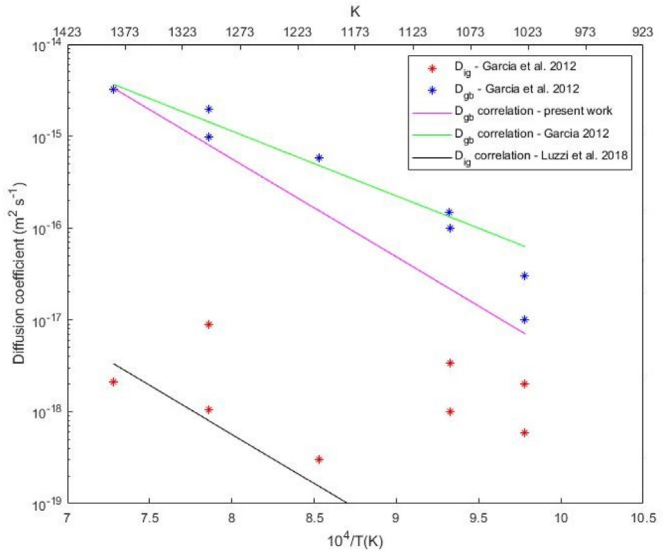

Fig. 6. Helium diffusion coefficients within the grain (red data) and around the grain boundaries (blue data) [30]. Different correlation are reported on the graph: the correlation proposed for grain boundary diffusion in the samples studied by Garcia et al. (green line), the correlation adopted for grain boundary helium in this work (purple line) and the correlation adopted in the intra-granular helium model [22,37]. (For interpretation of the references to colour in this figure legend, the reader is referred to the Web version of this article.)

[1] Another potential process which could be invoked to explain helium release at relatively low temperatures is related to the presence of helium in fabrication porosities which are or rapidly become open during the annealing test. This aspect is disregarded in the present work because in the considered validation dataset the fabrication porosity and its open fraction is not characterized.

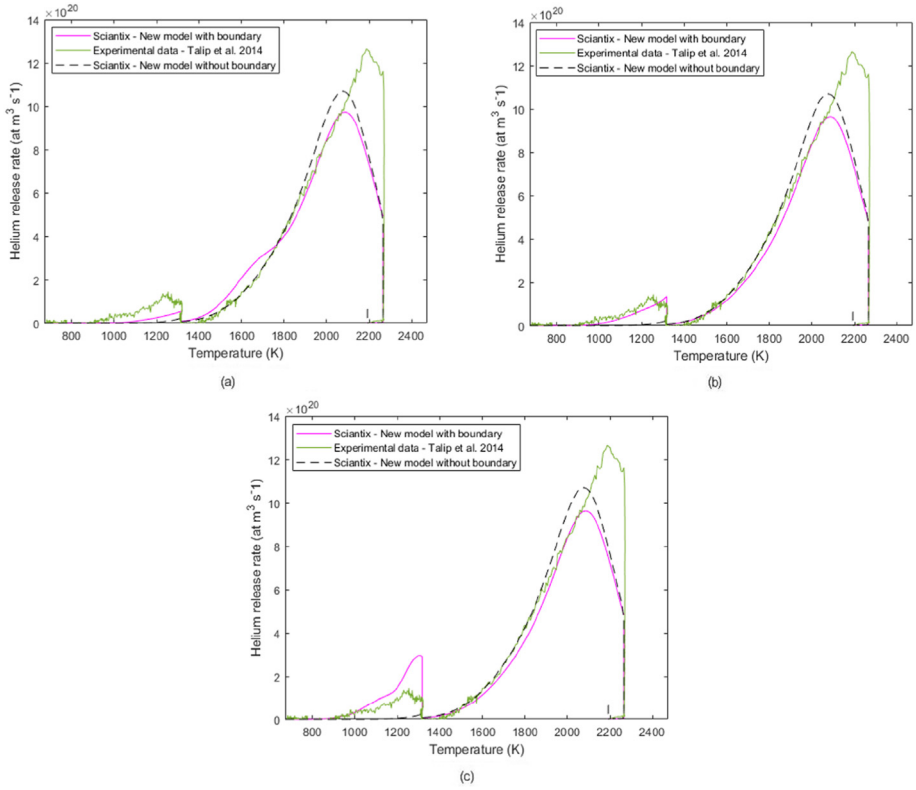

Fig. 7. Example of the Effect of different values of Diffusion ratio on helium release rate for the 1320 K history: (a) $D_{gb}/D_{ig} = 10^2$, (b) $D_{gb}/D_{ig} = 10^3$, (c) $D_{gb}/D_{ig} = 10^4$.

uncertainty on the final release will be more marked for the history at 1400 K (short) and substantially negligible for those stories (1320 K and 1400 K) in which the maximum temperature achieved is between 2200 K and 2400 K, since at values this high all the helium in the samples (both intra-granular and inter-granular) is released anyway.

Concerning how helium at grain boundaries is initially split between inter-granular solution and inter-granular bubbles, it is relevant to see how this subdivision could impact the fractional release and the release rate. To understand the influence of the aforementioned division, the behaviour determined by the annealing history at 1800 K is considered (Figs. 2(e) and Fig. 3(e)). Since no assessed data are available, this case also required a proper uncertainty analysis. The fraction of helium in the inter-granular bubbles is varied in a range between 0% and 50% of the total helium initially present at grain boundaries. Fig. 5(c) and (d) show that the initial helium distribution has a negligible impact on the overall fractional release, but it results in some changes on the first peak in helium release rate. This is reasonably within expectations, since the helium distribution in bubble and single-atom concentrations does not affect how much helium is ultimately released (the integral of the release is not affected), while, on the other hand, having more helium in bubbles at the initial stages of release means that more gas needs to return in solution before release, slightly reducing the rate and vice versa (the release rate is what perceives the effect of the split). This effect is then reflected on the first peak because it is the one associated to the release of helium initially present at grain boundaries as stated above. Nevertheless, we can see that even along a 50% range of uncertainty the effect of this parameter is relatively small. Future data collection on this open issue could provide a more detailed insight on how this initial split should be treated.

Concerning the grain-boundary diffusion coefficient D_{gb}, one would expect a pre-exponential term and an activation energy typical for an Arrhenius form. Nevertheless, the lack of experimental data for this specific case and the large scatter, led to the choice of considering the same diffusion correlation adopted by Cognini et al. [22] in the intra-granular only version of this model, but increased by a certain factor defined by the ratio D_{gb}/D_{ig} [30]. This reduces the number of parameters for the grain boundary diffusion to one ratio.

The interesting results obtained by Garcia et al. [30] are presented in Fig. 6, that shows values at different temperatures of the helium intra-granular and inter-granular diffusion coefficient in UO_2 polycrystalline samples. From those results, it is possible to evaluate the diffusion ratio. Comparing the intra-granular and inter-granular experimental data reported in Fig. 6 it is possible to determine that the diffusion ratio varies in a range between $D_{gb}/D_{ig} \sim 10^2$ and $D_{gb}/D_{ig} \sim 10^4$. At the highest temperature at which data were collected (1373 K), the value of the ratio is $D_{gb}/D_{ig} \sim 10^3$. Since this last value of the ratio is achieved at a temperature that is the closest (among the ones in Fig. 6) to the holding temperature of the annealing history considered, it is assumed as the reference value for the diffusion ratio adopted in this work.

We can see from Fig. 5(b) that the impact of the diffusion coefficient uncertainty on the final fractional helium release is basically negligible for the temperature histories considered. The impact of the diffusion coefficient is more significant on the helium release rate. As we can see from Fig. 7 the effect of different values for the diffusion ratio (showed on the 1320 K history) affects the “shape” of the first peak of the release rate, which is expected since it is the one attributable to the release of inter-granular helium. This effect is due to the fact that, given the dependency on temperature of the diffusion coefficient, a smaller value for the ratio (i.e., a smaller inter-granular diffusivity) causes the release from the grain-boundary to occur at higher temperatures, thus lowering the first peak and delaying grain boundary release. On the other hand,

if the value of the ratio increases, then the peak appears higher and earlier due to the release occurring at lower temperatures. In Fig. 7(a) and (c) it can be observed a change in the slope of the release rate curves, occurring during the high and low temperature peaks, respectively. This change in slope is ascribed to the relative weight of the competing process of trapping and thermal re-solution, characterized by different activations energy (see Table 1) and thus presenting different slopes of the helium release rate as function of temperature.

5. Conclusion

In this work, a new model for the description of inter-granular helium behaviour is proposed. The model is implemented in SCIANTIX and aims at improving the predictive capabilities on the helium behaviour by including a description of helium evolution at grain boundaries.

The model is compared with a set of data collected during annealing experiments on UO_2 samples doped with ^{238}Pu as α-emitter. The results show that the inclusion of a model treating helium behaviour at grain boundaries generally improves the predictions with respect to the early works, lacking the inter-granular helium diffusion. This improvement is well appreciated on the release rate of the annealing performed at a constant temperature of 1800 K, where the experimentally observed double peak, previously absent in the state-of-the-art predictions, becomes visible and is captured as driven by release of helium stored at the grain boundaries. The presented validation dataset is obtained at the JRC and is limited to fuel temperatures that are higher than those expected in dry storage conditions, hence further investigation in this low temperature (below 650 K) regime is to be performed.

The uncertainty analysis on some critical parameters (grain-boundary helium diffusivity and initial concentration of helium at the grain boundary) showed that, within a reasonable range, they bear negligible impact on the final value of the release and on the kinetics of release rate. This corroborates the reliability of the presented validation results but should not be generalized outside of the current validation of the model.

Several future developments are planned to overcome current model limitations. Further investigations on the distribution of the grain-boundary helium among in-bubble and single-atom concentrations can improve the model predictions. A more detailed experimental knowledge would improve the quality of our assumptions. The definition of a proper grain-boundary diffusion coefficient (rather than a ratio with respect to the intra-granular diffusivity) would also improve a more precise evaluation of the diffusion process from the grain boundaries. Lastly, the model for helium should also be coupled with the model for inert gas atoms for the simulation of nuclear fuel during irradiation by means of SCIANTIX.

Declaration of competing interest

The authors declare that they have no known competing financial interests or personal relationships that could have appeared to influence the work reported in this paper.

Acknowledgements

This work has received funding from the Euratom research and training programme 2019–2020 under grant agreement No 945077 (PATRICIA Project).

References

[1] T. Wiss, et al., Evolution of spent nuclear fuel in dry storage conditions for millennia and beyond, J. Nucl. Mater. 451 (1–3) (2014) 198–206.
[2] P. Konarski, C. Cozzo, G. Khvostov, H. Ferroukhi, Spent nuclear fuel in dry storage conditions – current trends in fuel performance modeling, J. Nucl. Mater. 555 (2021) 153138.
[3] M.G. El-Samrah, A.F. Tawfic, S.E. Chidiac, Spent nuclear fuel interim dry storage; Design requirements, most common methods, and evolution: a review, Ann. Nucl. Energy 160 (2021) 108408.
[4] J.S. Kim, J.D. Hong, Y.S. Yang, D.H. Kook, Rod internal pressure of spent nuclear fuel and its effects on cladding degradation during dry storage, J. Nucl. Mater. 492 (2017) 253–259.
[5] G. Spykman, Dry storage of spent nuclear fuel and high active waste in Germany - current situation and technical aspects on inventories integrity for a prolonged storage time, Nucl. Eng. Technol. 50 (2) (2018) 313–317.
[6] H.J. Cha, K.N. Jang, K.T. Kim, An allowable cladding peak temperature for spent nuclear fuels in interim dry storage, J. Nucl. Mater. 498 (2018) 409–420.
[7] S. Alyokhina, Thermal analysis of certain accident conditions of dry spent nuclear fuel storage, Nucl. Eng. Technol. 50 (5) (2018) 717–723.
[8] P.A.C. Raynaud, R.E. Einziger, Cladding stress during extended storage of high burnup spent nuclear fuel, J. Nucl. Mater. 464 (2015) 304–312.
[9] A. Arkoma, R. Huhtanen, J. Leppänen, J. Peltola, T. Pättikangas, Calculation chain for the analysis of spent nuclear fuel in long-term interim dry storage, Ann. Nucl. Energy 119 (2018) 129–138.
[10] P. Van Uffelen, C. Győri, A. Schubert, J. van de Laar, Z. Hózer, G. Spykman, Extending the application range of a fuel performance code from normal operating to design basis accident conditions, J. Nucl. Mater. 383 (1–2) (2008) 137–143.
[11] F. Feria, L.E. Herranz, J. Penalva, On the way to enabling FRAPCON-3 to model spent fuel under dry storage conditions: the thermal evolution, Ann. Nucl. Energy 85 (2015) 995–1002.
[12] L.E. Herranz, J. Penalva, F. Feria, CFD analysis of a cask for spent fuel dry storage: the thermal evolution, Ann. Nucl. Energy 76 (2015) 54–62.
[13] D. Pizzocri, et al., A model describing intra-granular fission gas behaviour in oxide fuel for advanced engineering tools, J. Nucl. Mater. 502 (2018) 323–330.
[14] G. Pastore, L. Luzzi, V. Di Marcello, P. Van Uffelen, Physics-based modelling of fission gas swelling and release in UO_2 applied to integral fuel rod analysis, Nucl. Eng. Des. 256 (2013) 75–86.
[15] T. Barani, et al., Analysis of transient fission gas behaviour in oxide fuel using BISON and TRANSURANUS, J. Nucl. Mater. 486 (2017) 96–110.
[16] G. Pastore, et al., Uncertainty and sensitivity analysis of fission gas behavior in engineering-scale fuel modeling, J. Nucl. Mater. 456 (2015) 398–408.
[17] T. Wiss, et al., Properties of the high burnup structure in nuclear light water reactor fuel, Radiochim. Acta 105 (11) (2017) 893–906.
[18] D. Pizzocri, F. Cappia, L. Luzzi, G. Pastore, V.V. Rondinella, P. Van Uffelen, A semi-empirical model for the formation and depletion of the high burnup structure in UO_2, J. Nucl. Mater. 487 (2017) 23–29.
[19] K. Lassmann, TRANSURANUS: a fuel rod analysis code ready for use, J. Nucl. Mater. 188 (C) (1992) 295–302.
[20] B. Baurens, J. Sercombe, C. Riglet-Martial, L. Desgranges, L. Trotignon, P. Maugis, 3D thermo-chemical-mechanical simulation of power ramps with ALCYONE fuel code, J. Nucl. Mater. 452 (1–3) (2014) 578–594.
[21] J.D. Hales, R.L. Williamson, S.R. Novascone, G. Pastore, B.W. Spencer, D.S. Stafford, K.A. Gamble, D.M. Perez, W. Liu, BISON Theory Manual - the Equations behind Nuclear Fuel Analysis, Idaho Falls, 2016.
[22] L. Cognini, A. Cechet, T. Barani, D. Pizzocri, P. Van Uffelen, L. Luzzi, Towards a physics-based description of intra-granular helium behaviour in oxide fuel for application in fuel performance codes, Nucl. Eng. Technol. 53 (2021) 562–571.
[23] H.J. Matzke, Gas release mechanisms in UO_2 - a critical review, Radiat. Eff. 53 (3–4) (1980) 219–242.
[24] M.S. Veshchunov, On the theory of fission gas bubble evolution in irradiated UO_2 fuel, J. Nucl. Mater. 277 (2000) 67–81.
[25] D.R. Olander, D. Wongsawaeng, Re-solution of fission gas – a review: Part I. Intragranular bubbles, J. Nucl. Mater. 354 (1–3) (2006) 94–109.
[26] M. Tonks, et al., Unit mechanisms of fission gas release: current understanding and future needs, J. Nucl. Mater. 504 (2018) 300–317.
[27] J. Rest, M.W.D. Cooper, J. Spino, J.A. Turnbull, P. Van Uffelen, C.T. Walker, Fission gas release from UO_2 nuclear fuel: a review, J. Nucl. Mater. 513 (2019) 310–345.
[28] R.J. White, The development of grain-face porosity in irradiated oxide fuel, J. Nucl. Mater. 325 (1) (2004) 61–77.
[29] D. Pizzocri, T. Barani, L. Luzzi, SCIANTIX: a new open source multi-scale code for fission gas behaviour modelling designed for nuclear fuel performance codes, J. Nucl. Mater. 532 (2020) 152042.
[30] P. Garcia, et al., A study of helium mobility in polycrystalline uranium dioxide, J. Nucl. Mater. 430 (1–3) (2012) 156–165.
[31] P. Van Uffelen, Contribution to the Modelling of Fission Gas Release in Light Water Reactor Fuel, 2002. PhD Thesis.
[32] D.R. Olander, P. Van Uffelen, On the role of grain boundary diffusion in fission gas release, J. Nucl. Mater. 288 (2–3) (2001) 137–147.
[33] P. Van Uffelen, Modelling the variable precipitation of fission products at grain boundaries, J. Nucl. Mater. 280 (3) (2000) 275–284.

[34] A.M. Booth, A Method of Calculating Fission Gas Diffusion from UO_2 Fuel and its Application to the X-2-F Loop Test, 1957.
[35] L. Cognini, et al., Helium solubility in oxide nuclear fuel: derivation of new correlations for Henry's constant, Nucl. Eng. Des. 340 (2018) 240–244.
[36] Z. Talip, et al., Thermal diffusion of helium in 238Pu-doped UO_2, J. Nucl. Mater. 445 (1–3) (2014) 117–127.
[37] L. Luzzi, et al., Helium diffusivity in oxide nuclear fuel: critical data analysis and new correlations, Nucl. Eng. Des. 330 (2018).
[38] D.R. Olander, Fundamental Aspects of Nuclear Reactor Fuel Elements, 1976.
[39] K. Nakajima, H. Serizawa, N. Shirasu, Y. Haga, Y. Arai, The solubility and diffusion coefficient of helium in uranium dioxide, J. Nucl. Mater. 419 (1–3) (2011) 272–280.
[40] F. Rufeh, D.R. Olander, T.H. Pigford, The solubility of helium in uranium dioxide, Nucl. Sci. Eng. 23 (4) (1965) 335–338.
[41] E. Maugeri, et al., Helium solubility and behaviour in uranium dioxide, J. Nucl. Mater. 385 (2) (2009) 461–466.
[42] L. Van Brutzel, A. Chartier, A new equation of state for helium nanobubbles embedded in UO_2 matrix calculated via molecular dynamics simulations, J. Nucl. Mater. 518 (2019) 431–439.
[43] R.M. Davies, S.G. Taylor, The mechanics of large bubbles rising through extended liquids and through liquids in tubes, Dyn. Curved Front. 200 (1062) (1988) 377–392.
[44] J.Y. Colle, et al., A mass spectrometry method for quantitative and kinetic analysis of gas release from nuclear materials and its application to helium desorption from UO_2 and fission gas release from irradiated fuel, J. Nucl. Sci. Technol. 51 (5) (2014) 700–711.
[45] G. Martin, et al., Helium release in uranium dioxide in relation to grain boundaries and free surfaces, Nucl. Instrum. Methods Phys. Res. Sect. B Beam Interact. Mater. Atoms 268 (11–12) (2010) 2133–2137.
[46] G. Martin, et al., A quantitative μNRA study of helium intergranular and volume diffusion in sintered UO_2, Nucl. Instrum. Methods Phys. Res. Sect. B Beam Interact. Mater. Atoms 249 (1–2 SPEC. ISS.) (2006) 509–512.